Biomolecule-inspired synthesis of framework zinc in MFI zeolite for propane dehydrogenation

Xunming Su [a,b], Zhong-Pan Hu [b,c], Jingfeng Han [b,c], Yuhong Jia [b,c], Shutao Xu [b,c], Jin Zhang [b,c], Dong Fan [b,c], Yingxu Wei [b,c,**], Zhongmin Liu [a,b,c,*]

[a] School of Chemistry and Materials Science, University of Science and Technology of China, Hefei, Anhui, 230026, China
[b] National Engineering Research Center of Lower-Carbon Catalysis Technology, Dalian National Laboratory for Clean Energy, iChEM Collaborative Innovation Center of Chemistry for Energy Materials, Dalian Institute of Chemical Physics, Chinese Academy of Sciences, Dalian, 116023, China
[c] State Key Laboratory of Catalysis, Dalian Institute of Chemical Physics, Chinese Academy of Sciences, Dalian, 116023, China

ARTICLE INFO

ABSTRACT

The development of environment-friendly, stable, and efficient catalysts to substitute Pt and Cr-based catalysts for propane dehydrogenation (PDH) is of great importance but challenging to make. Herein, we use zinc gluconate ($Zn(C_6H_{12}O_7)_2$), an organometallic biomolecule, to embed Zn atoms into pure silica MFI zeolite framework (Zn-MFI) for PDH reaction. Due to the protection by the glucosyl groups in $Zn(C_6H_{12}O_7)_2$, Zn atoms can be well embedded into the MFI zeolite framework. Multi-scale characterizations (*e.g.*, C_s-corrected HAADF-STEM, FTIR, UV–vis, and NMR spectroscopy) and DFT calculations demonstrate the formation of uniform tetrahedrally coordinated Zn sites in the MFI zeolite framework with two Zn–O–Si and two Zn···OH–Si linkages ($\{(\equiv SiO)_2Zn(HO-Si\equiv)_2\}$). The Zn-MFI zeolites are used for PDH, exhibiting excellent catalytic performance. Pyridine-FTIR, C_3H_6-FTIR, C_3H_6-TPD/MS, and contrast experiments reveal the unique Zn active sites in Zn-MFI zeolites can promote the C–H bond cleavage and weaken the propylene adsorption, thus guaranteeing high activity and selectivity for PDH. The excellent catalytic performance of Zn-MFI zeolites indicates their promising utilization in industry.

1. Introduction

Propane dehydrogenation to propylene is one of the economical processes for propylene production due to its short process flow, low carbon emissions, and increased production of propane from shale gas. The direct dehydrogenation of propane (PDH) to propylene and H_2 is a thermodynamically limited endothermic process. To decrease the thermodynamic limitations and increase the catalyst lifespan, an oxidizing agent such as O_2 and CO_2 is introduced into the alkane dehydrogenation process, namely the oxidation dehydrogenation (ODH) process. However, due to the deep oxidation of reactants and products, the ODH process suffers from low olefin selectivity, which has not been commercialized yet [1–3].

Direct propane dehydrogenation can be catalyzed by supported metal or metal oxide catalysts. supported Pt- and Cr-based catalysts have been widely used in industrial PDH processes, *i.e.*, Catofin and Oleflex

crafts [4–6]. However, the Pt- and Cr-based catalysts suffer from intractable problems in terms of high cost and environmental toxicity. The development of alternative catalysts with cheap and environment-friendly features for the PDH process has attracted great attention [7]. Over the past several decades, many novel catalysts have been exploited for alkane dehydrogenation, such as VO_x, GaO_x, ZrO_x, ZnO_x, carbides, nitrides, and carbon materials [8–13]. Among these catalysts, Zn-based materials represent a kind of promising catalyst for alkane dehydrogenation owing to their low cost and environment-friendly properties [7,11,14]. With the in-depth investigation of Zn-based catalysts, it was found that the Zn sites located on diverse supports possessed different coordinated structures, which exhibited very different catalytic performances for alkane dehydrogenation [10,15,16]. For example, Hock and co-workers reported that the Zn/SiO_2 catalyst synthesized by the electrostatic adsorption method possessed tetrahedrally coordinated Zn sites which could transform into

---

3-coordinated active centers and exhibited high propylene selectivity during PDH [17]. However, the Zn sites possess weak interactions with the SiO$_2$ support, which would be easily aggregated into ZnO particles and result in rapid deactivation during PDH.

To improve the catalytic performance of Zn-based catalysts, several recent studies were performed to introduce Zn species into zeolites [20–26]. Zeolite can provide a unique structure and microenvironment to modify the coordinated and electronic structure of the metal species, making them particularly beneficial for alkane dehydrogenation [18, 19]. For instance, Zn ions introduced into HZSM-5 zeolite (Zn/HZSM-5) by ions exchange and incipient wetness impregnation methods were reported to be active for PDH. In the Zn/HZSM-5 zeolites, Zn ions interacted with two framework oxygen atoms or formed as [ZnOH]$^+$ species were proposed as the active sites [20–22]. However, ZnO clusters and nanoparticles would be easily formed on the HZSM-5 zeolite since most Zn ions could not transfer into the channels of zeolite during the ions exchange or incipient wetness impregnation processes [23–26]. Furthermore, the Brønsted acid sites in HZSM-5 would lead to cracking,

deep dehydrogenation, and aromatization reactions. It is known that the introduction of Zn atoms into the zeolite framework is of great importance but challenge to make. Over the past several years, many methods have been developed for the synthesis of framework Zn-based zeolite. For example, Zn-Beta zeolites have been prepared by an improved two-step post-synthesis method, which consists of creating vacant sites with associated silanol groups by dealumination H-Beta and subsequently impregnation of Si-Beta with Zn precursors [27,28]. Also, the hydrothermal synthesis method using ethylenediamine coordinated zinc acetate dihydrate (Zn(NH$_2$CH$_2$CH$_2$NH$_2$)$_3$(OAc)$_2$) has been exploited for the synthesis of Zn@S-1 zeolite. However, a number of ZnO clusters or nanoparticles would be formed during these methods owing to the lability of the metal precursor in solution conditions [29,30]. Recently, Kondratenko and co-workers designed a H$_2$-reduction method to embed Zn atoms into silicalite-1 zeolites by reducing ZnO and silicalite-1 mixture in a high-temperature H$_2$ atmosphere [31]. Due to the mobility of Zn sites, binuclear −Zn–O–Zn− sites would be formed within the silicalite-1 zeolite, which is highly active for PDH reaction. Based on
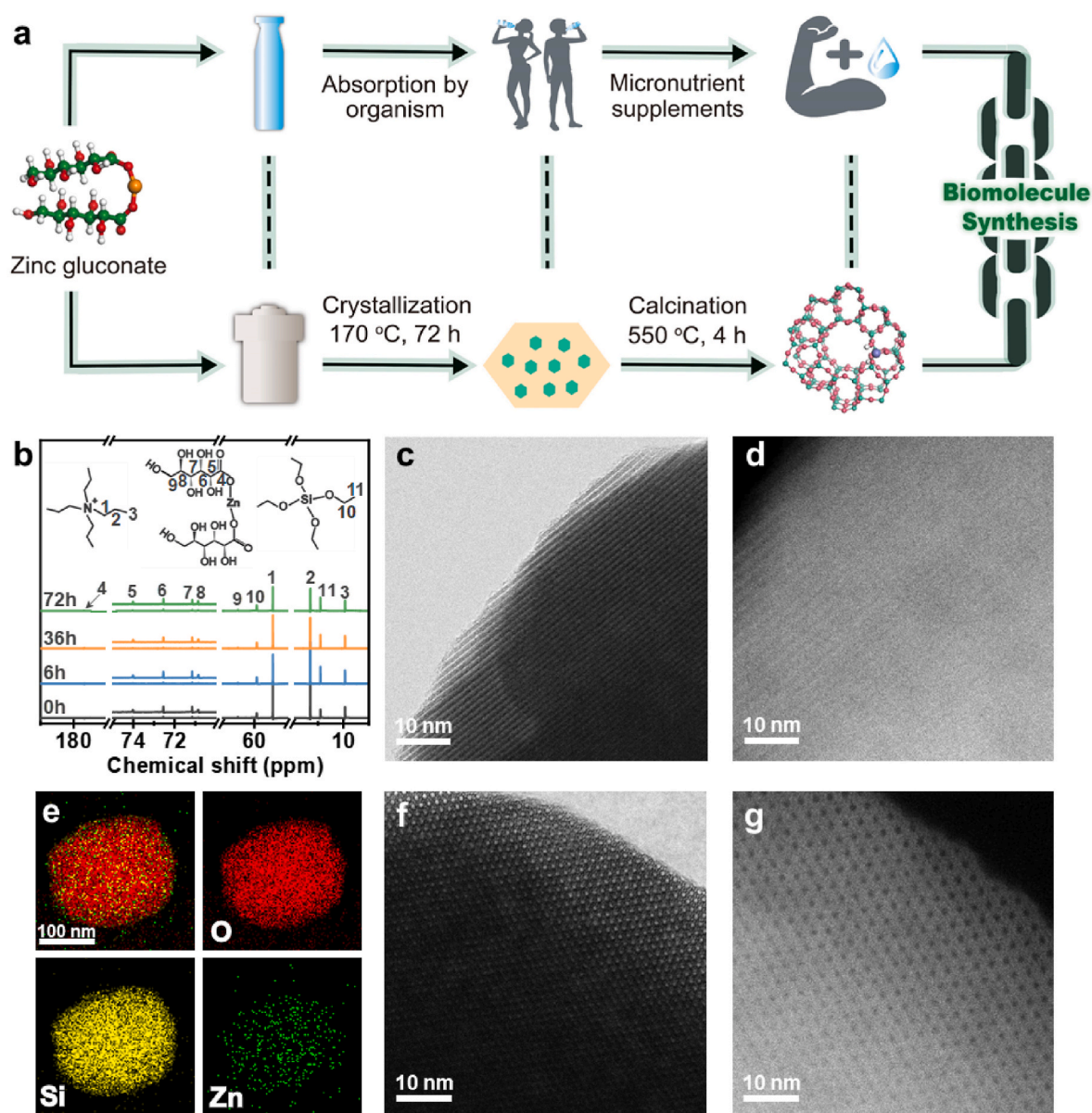

Fig. 1. (a) Schematic illustration of the biomolecule-inspired synthesis process for Zn-MFI zeolites. (b) Liquid ^{13}C NMR of synthesis gels at various crystallization times (0, 6, 36, and 72 h), and the spectra analysis is based on the website of SDBS (AIST). (c, f) C$_s$-corrected TEM and (d, g) HAADF-STEM images of 2.0%Zn-MFI zeolite. (e) EDS elemental mapping images of 2.0%Zn-MFI zeolite (O, Si, and Zn).

the above study, it can be found that Zn sites incorporated into the zeolite framework or attached to the silanol nests of zeolites exhibit high alkane dehydrogenation performance. Some previous research has reported that organometallic precursors (*e.g.,* diethylzinc, bis(2, 4-dimethyl-1,3-pentadienide) iron(II), and ($\equiv$SiO)$_2$V^V(O)Mes (Mes = 2,4,6-trimethylphenyl)) can be used to synthesize isolated metal sites onto SiO$_2$ and Al$_2$O$_3$ supports [16,32,33].

In this work, we use zinc gluconate firstly to incorporate Zn atoms into the pure silica MFI zeolite framework (Zn-MFI). Owing to the high solubility and good stability of zinc gluconate in alkaline and hydrothermal conditions, resulting in Zn atoms can be well incorporated into the MFI zeolite framework. The synthesized Zn-MFI zeolites possess good crystallinity and homogeneous isolated Zn sites in the MFI zeolite framework, which exhibit excellent catalytic performance for PDH. The structural and chemical properties of the isolated Zn sites are characterized and illustrated by various characterizations and density functional theory (DFT) calculations, revealing the unique Zn sites with two Zn–O–Si and two Zn$\cdots$OH–Si linkages are particularly beneficial for PDH reaction.

2. Results and discussion

Zinc gluconate (Zn(C$_6$H$_{11}$O$_7$)$_2$) is a typical nutrient for the human body, ensuring normal skeletal growth and bone homeostasis. Zinc gluconate has a higher solubility and bioavailability than inorganic zinc because the organic branches prevent the formation of insoluble complexes of zinc ions in the gastrointestinal tract [34]. Herein, inspired by the human body absorption of zinc ions from zinc gluconate, we incorporate Zn sites into the MFI zeolite framework (Zn-MFI) using zinc gluconate as the metal precursor (Fig. 1a). Typically, the Zn-MFI zeolites are synthesized in gel systems with the molar compositions of 1.0SiO$_2$:0.4TPAOH (tetrapropylammonium hydroxide):35H$_2$O:aZn (C$_6$H$_{11}$O$_7$)$_2$ (a = 0.014, 0.018 and 0.028) under hydrothermal conditions at 170 °C for 72 h. After calcination, Zn-MFI zeolites with different Zn contents can be obtained (Table S1). The powder X-ray diffraction (PXRD) patterns show that all the Zn-MFI samples possess typical diffraction peaks for MFI topological structure (Fig. S1). The enlarged XRD patterns from 23.0° to 25.0° show that the diffraction peaks of Zn-MFI shift to the lower angle as compared to those of silicalite-1. This is due to the isomorphous substitution of tetrahedral Si atoms (Si–O band, 1.62 Å) by Zn atoms (Zn–O band, 1.95 Å) [35,36]. The FTIR spectra of silicalite-1 and 2.0%Zn-MFI zeolites are shown in Fig. S2. Apart from the typical bands of the MFI zeolite structure at 445, 549, 796, and 1224 cm^{-1}, the silicalite-1 zeolite exhibits a band at 1106 cm^{-1}, which can be attributed to the asymmetric stretching of T-O band of zeolite framework. After introducing 2 wt% Zn in the MFI zeolite framework, the asymmetric stretching of the T-O band shifts to a lower frequency (1101 cm^{-1}). The FTIR result demonstrates that in the Zn-MFI zeolite, the Si atoms in the Si–O–Si bands are replaced by the Zn atoms to form Zn–O–Si bands [36]. Scanning electron microscope (SEM) images and N$_2$ sorption results reveal the Zn-MFI zeolites are composed of uniform cubes with the size of ~200 nm (Fig. S3) and the specific surface areas of 390–400 m^2 g^{-1} (Fig. S4 and Table S1).

To understand the role of zinc gluconate in the formation of Zn-MFI zeolite, the synthesis gels with various crystallization times are characterized by the liquid ^{13}C nuclear magnetic resonance spectroscopy (^{13}C NMR, Fig. 1b). Clearly, the signals of TPAOH, zinc gluconate, and tetraethyl orthosilicate can be observed at different crystallization periods (0, 6, 36, and 72 h), suggesting the gluconate in zinc gluconate can prevent the Zn sites from precipitation during the whole crystallization process of Zn-MFI zeolite. The solid products are further investigated for different crystallization times (6, 36, and 72 h). Because only trace solid products are formed within 6 h, the solid products with crystallization times of 36 and 72 h are characterized by the XRD. The XRD pattern results show good MFI topological structure for the solid products at 36 and 72 h (Fig. S5). The thermogravimetric-differential thermal analysis

(TG/DTA) results show that the uncalcined silicalite-1 zeolite presents two weight loss steps in the temperature ranges of 30–250 and 350–400 °C, respectively (Fig. S6), corresponding to the evaporation of adsorbed water and the thermal decomposition of TPAOH, respectively [30]. As to the uncalcined Zn-MFI sample, an extra weight loss step is observed in the temperature range of 450–500 °C, which can be attributed to the decomposition of Zn(C$_6$H$_{11}$O$_7$)$_2$. This result is in good accordance with the liquid ^{13}C NMR spectra, suggesting that the Zn (C$_6$H$_{11}$O$_7$)$_2$ participates in the whole crystallization process.

The optimized Zn-MFI zeolite (Zn content, ~2.0%) is characterized by C$_s$-corrected high-angle annular darkfield scanning transmission electron microscopy (HAADF-STEM), showing a well-defined MFI structure (Fig. 1c, f and S7). Noticeably, no ZnO particles and aggregations can be observed over the Zn-MFI zeolite (Fig. 1d and g). The energy-dispersive X-ray spectroscopy (EDS) elemental mapping images of Zn-MFI verify the homogeneous distribution of Zn atoms (Fig. 1e).

Several characterizations are performed to clarify the coordinated structure and the homogeneity of Zn sites within the MFI framework. In Fig. 2a, the ultraviolet–visible (UV–vis) results show that the bulk ZnO displays a prominent peak at ~370 nm due to the electron transition from the valence band to the conduction band [37]. For Zn-MFI zeolite, the peaks at 250–400 nm are invisible in the UV–vis spectrum, indicating the absence of ZnO clusters or nanoparticles in the Zn-MFI channel. Notably, the weak peak at 190–200 nm is observed in the UV–vis spectrum of Zn-MFI, which is probably caused by the ligand-to-metal charge transfer transitions (*i.e.*, O^{2-} to Zn^{2+}), suggesting the isolated Zn sites are homogenously embedded into Zn-MFI zeolite framework [38]. When the Zn content increases to 3.1%, a broad peak at 250–400 nm can be observed (Fig. S8), indicating the formation of ZnO clusters or nanoparticles in the zeolite channel. The electronic states of Zn sites in Zn-MFI zeolite are characterized by X-ray photoelectron spectroscopy (XPS, Fig. S9). The Zn 2p XPS peak is so weak in Zn-MFI, probably because the isolated Zn sites are embedded into the zeolite framework [39,40]. The Zn-MFI possesses two peaks centered at 1022.6 and 1045.8 eV, respectively, which are assigned to the Zn 2p$_{1/2}$ and 2p$_{3/2}$ photoelectrons of Zn sites, respectively. The peaks of Zn 2p XPS in Zn-MFI shift to higher binding energies as compared with those of bulk ZnO (ΔE = 1.2 eV), which can be attributed to the electron transfer from the lower electronegativity of Zn to framework Si and thereby lead to a decrease valence electron density of Zn (Zn^{2+} to Si^{4+}) [36]. For comparison, 2.0%ZnA-MFI and 2.0%ZnN-MFI zeolite are synthesized using Zn(OAc)$_2$ and Zn(NO)$_3$ as metal precursors, respectively (Fig. S10 and Table S2). The UV–vis results exhibit a broad peak at ~370 nm, which is assigned to ZnO clusters or nanoparticles in ZnA-MFI and ZnN-MFI (Fig. S11). The above characterizations illustrate the utilization of zinc gluconate can embed Zn atoms into the MFI zeolite framework.

The hydroxyl groups in Zn-MFI zeolite are studied by diffuse reflectance infrared Fourier transforms spectroscopy (DRIFTS, Fig. 2b). After dehydration under vacuum at 450 °C, the Zn-MFI and silicalite-1 zeolites exhibit two bands at ~3725 and ~3532 cm^{-1}, respectively, which are assigned to the isolated silanol group and silanol nests, respectively [41]. The silicalite-1 has a high concentration of silanol nests and a low concentration of isolated silanol group. After the introduction of Zn atoms, the band at 3532 cm^{-1} decreased accompanied by an increase of the band at 3725 cm^{-1}, indicating the increase of isolated silanol groups and the decrease of silanol nests. The ^{29}Si magic-angle spinning nuclear magnetic resonance spectroscopy (^{29}Si MAS NMR) spectra of silicalite-1 and Zn-MFI are shown in Fig. S12. All these two spectra exhibit an intense and broad peak at −112 ppm, which is assigned to Q^4 species (Si(OSi)$_4$), while the shoulder at −102 ppm is attributed to Q^3 species (Si(OSi)$_3$(OH)) silicon atoms of silanol groups, suggesting most of the silicon in silicalite-1 and Zn-MFI zeolites exist as Si(OSi)$_4$. Furthermore, the ^{1}H–^{29}Si CP-MAS NMR spectra of silicalite-1 and Zn-MFI zeolites are provided in Fig. 2c. The intensity of the Q^3 peak at −102 ppm is dramatically improved. Moreover, two small ^{1}H–^{29}Si CP-MAS NMR peaks at −92 and −112 ppm can be observed,

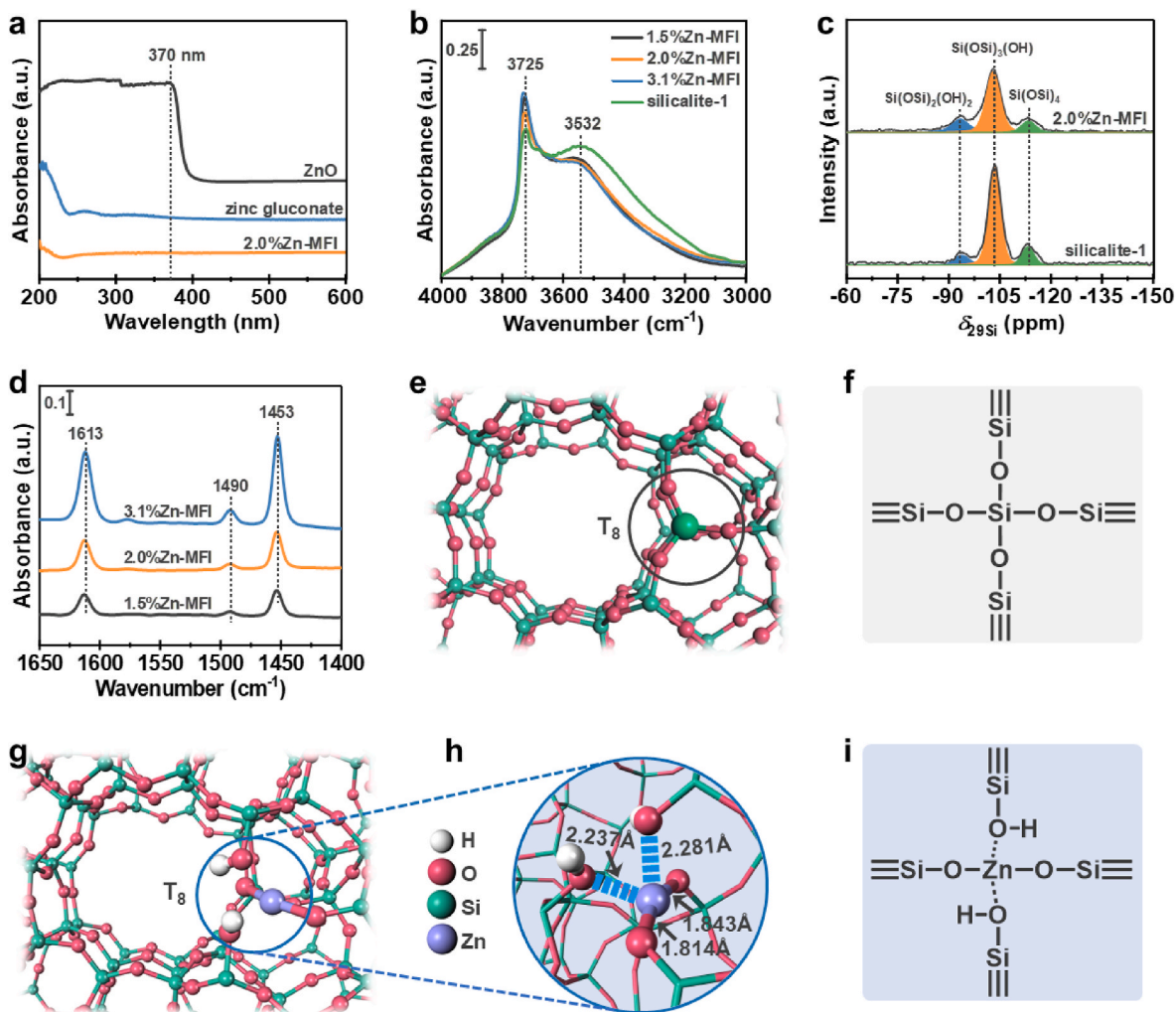**Fig. 2.** (a) UV–vis spectra of ZnO, $Zn(C_6H_{12}O_7)_2$, and 2.0%Zn-MFI samples. (b) DRIFTS spectra of 1.5%Zn-MFI, 2.0%Zn-MFI, 3.1%Zn-MFI, and silicalite-1 zeolites. (c) ^1H–^{29}Si CP MAS NMR spectra of silicalite-1 and 2.0%Zn-MFI zeolites. (d) FTIR spectra of 1.5%Zn-MFI, 2.0%Zn-MFI, and 3.1%Zn-MFI zeolites after pyridine adsorption and followed by evacuation at 100 °C. (e) The structure of silicalite-1 with Si atom at T_8 site by DFT calculations. (f) Schematic illustration of Si atom in silicalite-1 zeolite framework. (g) The structure of Zn-MFI with Zn atom at T_8 site by DFT calculations. (h) The distances between the Zn atom and the first coordinated O atoms. (i) Schematic illustration of Zn atom in the Zn-MFI zeolite framework.

which are assigned to Q^2 ($Si(OSi)_2(OH)_2$) and Q^4 species, respectively [42]. As compared to silicalite-1, the peak of Q^3 species decreases slightly after introducing Zn atoms into the MFI framework. Mintova and co-workers have reported that the incorporation of single W sites into the MFI zeolite could prevent the formation of silanol groups in W-MFI zeolite because the framework defects were saturated with W atoms coordinated with four or two Si atoms via oxygen bridges [43]. For Zn-MFI, the $Si(OSi)_3(OH)$ species still exist when Zn atoms are embedded into the MFI framework due to the Zn atoms cannot be directly coordinated with four Si atoms via oxygen bridges (Fig. 2c). Therefore, the increase of the band at 3725 cm^{-1} must be caused by the formation of Zn$\cdots$OH–Si linkages, and the decrease of the FTIR band at 3532 cm^{-1} is due to the formation of Zn–O–Si bands.

Density functional theory (DFT) calculations are performed to make clear the structure of Zn sites in the MFI framework. Three typical sites (T_8, T_{10}, and T_{12}) are molded and compared (Fig. 2e–i and S13). The Zn-MFI zeolite possesses a unique structure with two Zn–O–Si and two Zn$\cdots$OH–Si linkages. For instance, the Zn–O distances in Zn–O–Si bonds are 1.814 and 1.843 Å, while the Zn$\cdots$O distances in Zn$\cdots$OH–Si linkages are prolonged (2.237 and 2.281 Å) at T_8 site, which are very different to the silicalite-1 zeolite (Fig. 2e–i). This indicates that the incorporation of Zn atoms into the MFI framework result in a tetrahedrally coordinated

Zn atom with two Zn–O–Si and two Zn$\cdots$OH–Si linkages, {($\equiv$SiO)$_2$Zn(HO–Si$\equiv$)$_2$}. The special structure of Zn sites might be good for PDH reaction.

Furthermore, pyridine-FTIR experiments are performed to identify the acidity of Zn-MFI. All the Zn-MFI zeolites exhibit three bands at 1453, 1490, and 1613 cm^{-1} (Fig. 2d and S14), typical for Lewis acid sites. However, no characteristic bands about Brønsted acid sites (1640 and 1550 cm^{-1}) are detected in Zn-MFI [19,28,44]. In Zn-MFI, there are two Zn–O–Si and two Zn$\cdots$OH–Si linkages. The Zn sites can act as Lewis acid sites for pyridine adsorption, while the H in Zn$\cdots$OH–Si linkage cannot polarize pyridine to generate Brønsted acid sites [45,46]. Based on the above analysis, it can be concluded that the incorporation of Zn atoms into the MFI framework only result in the Lewis acidic sites located in the MFI zeolite framework.

When the isolated Zn sites are embedded into the MFI zeolite framework using zinc gluconate, the active Zn sites and the unique microenvironment of Zn-MFI might contribute together to propane activation and transformation. Typically, Zn-MFI zeolites exhibit steady conversion and high propylene selectivity over 600 min time on stream in PDH (Fig. 3a). The Zn content can affect the catalytic performance of Zn-MFI zeolites, *i.e.*, the initial propane conversions of Zn-MFI are 22.5% (1.5%Zn-MFI), 30.1% (2.0%Zn-MFI), and 39.4% (3.1%Zn-MFI),
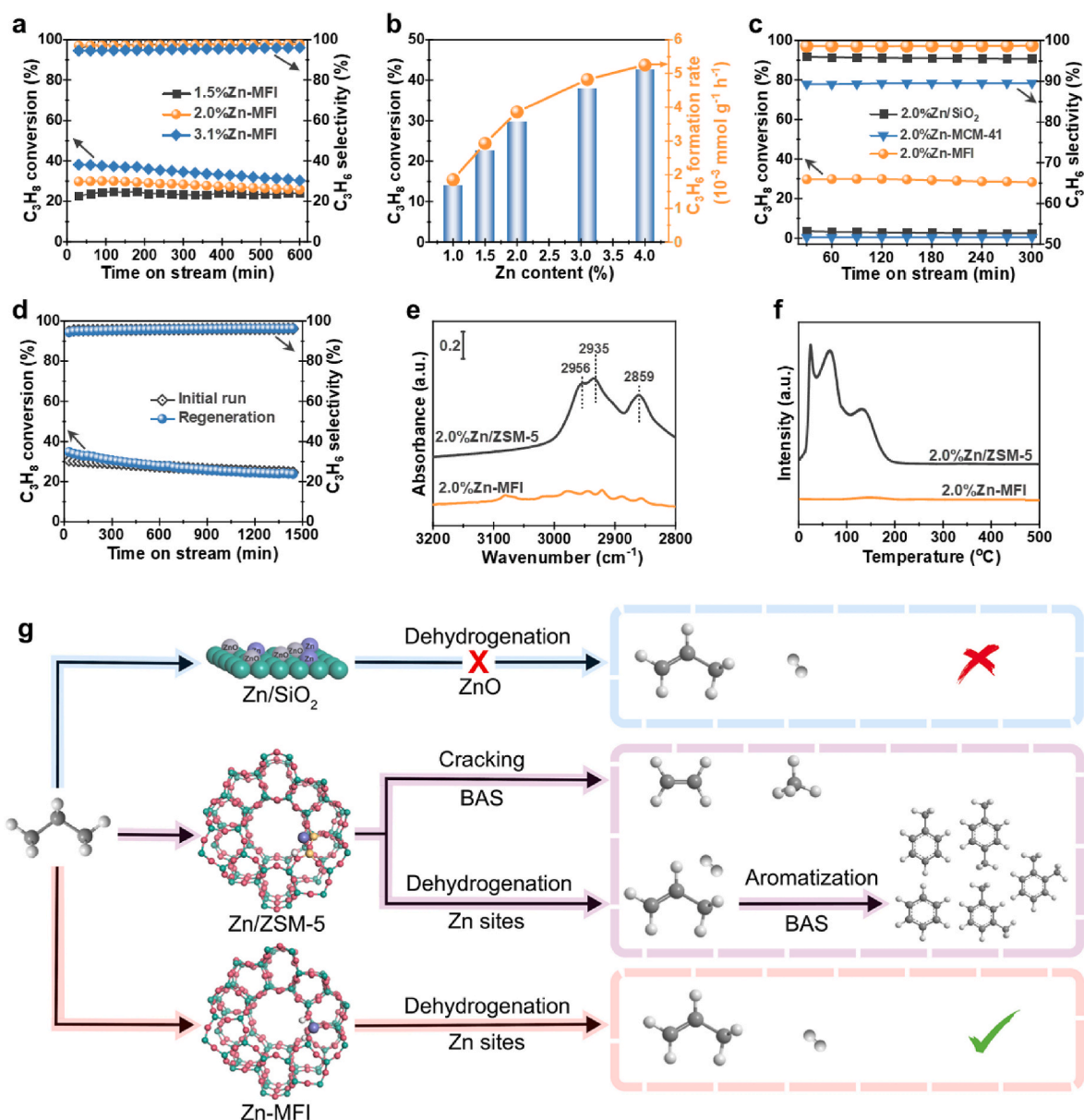
Fig. 3. (a) The propane conversion and propylene selectivity of Zn-MFI zeolites with time on stream. (b) The initial propane conversion and propylene formation rate of the Zn-MFI zeolites with different Zn contents (1.0%–4.1%). (c) The propane conversion and propylene selectivity of Zn/SiO$_2$, Zn-MCM-41, and Zn-MFI with time on stream. (d) Regeneration of 2.0%Zn-MFI zeolite in PDH reaction, regeneration conditions: the spent Zn-MFI is calcined in air flow (20 mL min^{-1}) at 550 °C for 30 min. (e) C$_3$H$_6$-FTIR spectra of 2.0%Zn-ZSM-5 and 2.0%Zn-MFI zeolites after adsorption of propylene and subsequently evacuation at 30 °C under Ar for 30 min. (f) C$_3$H$_6$-TPD/MS of 2.0%Zn-ZSM-5 and 2.0%Zn-MFI. (g) Schematic illustration of propane conversion on Zn/SiO$_2$, Zn/ZSM-5, and Zn-MFI. Reaction conditions: 0.2 g catalysts, atmospheric pressure, 5%C$_3$H$_8$/Ar, WHSV = 0.6 h^{-1}, 550 °C.

respectively. The 3.1%Zn-MFI exhibits a high activity but a lower propylene selectivity than 1.5%Zn-MFI and 2.0%Zn-MFI. According to the UV–vis results (Fig. S8), ZnO clusters and/or nanoparticles would be formed on 3.1%Zn-MFI. Therefore, secondary reactions such as aromatization and deep dehydrogenations would be occurred over 3.1% Zn-MFI owing to the Zn–O–Zn species. The effect of Zn content on the initial activity and propylene formation rate is further investigated (Fig. 3b). The propane conversion and propylene formation rate increase with the Zn content from 1.0% to 4.1%. At low Zn content <2.0%, the propane conversion and propylene formation rate show a good linear relationship to the Zn content. Further increasing the Zn content to 4.1% would result in a low increasing rate for propane conversion and propylene formation rate. This trend is in good accordance with the UV–vis results, indicating the formation of ZnO clusters or nanoparticles in Zn-MFI at high Zn content of over 2.0%. This also suggests the ZnO clusters

or nanoparticles in Zn-MFI are inactive for PDH reaction.

For comparison, Zn/SiO$_2$ and Zn-MCM-41 are synthesized and tested for PDH, showing much lower propane conversion than Zn-MFI (Fig. 3c), *i.e.*, 5.0% (Zn/SiO$_2$) and 3.0% (Zn-MCM-41). Due to the lack of confinement effect in SiO$_2$ and MCM-41 supports, ZnO particles would be formed and exhibit low PDH performance. Moreover, the catalytic performance of the previous Zn-based and other metal-based catalysts are listed in Table S3. Notably, the initial propane conversion of Zn-MFI is 30.1% and propylene selectivity is 97.5%, which is comparable to that of Zn-based and Cr-based catalysts, illustrating the excellent PDH performance. In Fig. 3d, the long-term stability of Zn-MFI is provided, showing high activity and stability for 1440 min time on stream. After regeneration, a high propane conversion and propylene selectivity can be obtained, suggesting the good stability of Zn-MFI zeolite. TG/DTA analysis of the spent Zn-MFI catalyst after 24 h time

on stream shows a weight loss of 0.45% in the temperature range of 450–600 °C (Fig. S15), indicating the strong anti-coking property of Zn-MFI. According to the pyridine-FITR (Fig. 2d) and DFT calculations (Fig. 2g–i), the Zn atom possesses relatively weak interactions to O atoms in Zn⋯OH–Si linkages and only result in Lewis acid sites. Therefore, side reactions owing to the Brønsted acid sites can be avoided, guaranteeing high activity, selectivity, and stability for PDH.

To further illustrate the excellent PDH performance of Zn-MFI, C_3H_6-FTIR and C_3H_6-TPD characterizations are performed. In Fig. 3e, the FTIR spectrum of Zn/ZSM-5 shows three bands at 2859, 2935, and 2956 cm^{-1}, corresponding to the propylene absorbed on the zeolite surface [47]. However, only very weak bands can be observed over the Zn-MFI, suggesting the presence of weak interactions between propylene and Zn-MFI zeolite. Thus, the generated propylene can quickly leave the catalyst and avoid secondary reactions. Also, the C_3H_6-TPD/MS desorption result of Zn-MFI shows almost no propylene desorption signal (Fig. 3f), further confirming the presence of weak interactions between propylene and Zn-MFI zeolite. Based on the above characterizations and analysis, it can be concluded that the Zn-MFI zeolites synthesized using zinc gluconate possess good crystallinity and isolated Zn species into the MFI zeolite framework. The electronic and structural properties of metal sites are significantly modified by the zeolite framework, making them highly active for alkane dehydrogenation [31, 48,49].

In Fig. 3g, we propose the possible catalytic processes for different Zn-based catalysts. For Zn/SiO$_2$, the Zn ions loading on the silica surface result in ZnO particles due to the presence of weak metal-support interactions, which leads to low PDH performance [16]. As to Zn/HZSM-5, the Brønsted acid sites in H-ZSM-5 would result in propane cracking, oligomerization, and aromatization, which are negative for PDH reaction [50]. When Zn atoms are introduced into the pure silica MFI zeolite framework, tetrahedrally coordinated Zn sites ({(≡SiO)$_2$Zn(HO–Si≡)$_2$} with two Zn–O–Si and two Zn⋯OH–Si linkages) would be formed in the Zn-MFI, which are highly active for PDH reaction. Previously, we have demonstrated that the Co-MFI with {(≡SiO)$_2$Co(HO–Si≡)$_2$} structure exhibited high catalytic performance for PDH due to the fact that the isolated Co-motif together with MFI microenvironment collectively promotes the PDH process [19]. In this work, zinc gluconate (Zn $(C_6H_{12}O_7)_2$) as a precursor can embed isolated tetrahedral Zn atoms into the MFI zeolite framework, forming similar microstructure and microenvironment to those of Co-MFI zeolite. The unique Zn sites in the form of {(≡SiO)$_2$Zn(HO–Si≡)$_2$} and the surrounding microenvironment can synergistically accelerate the PDH process.

3. Conclusions

In summary, we conduct a concise hydrothermal synthesis method to embed isolated Zn atoms into the MFI zeolite framework using zinc gluconate (Zn($C_6H_{12}O_7$)$_2$). Owing to the solubility and good stability of zinc gluconate in alkaline and hydrothermal conditions, Zn atoms can be well incorporated into the MFI zeolite framework. The C_s-HAADF-STEM images and UV–vis spectra demonstrate that the Zn atoms are homogeneously dispersed throughout the MFI framework. FTIR, XPS, ^{1}H–^{29}Si CP NMR analyses, and DFT theoretical calculations confirm the formation of tetrahedrally coordinated Zn sites with two Zn–O–Si and two Zn⋯OH–Si linkages, {(≡SiO)$_2$Zn(HO–Si≡)$_2$}. In particular, the Zn–O interactions in Zn⋯OH–Si linkages are so weak and only result in Lewis acid sites.

C_3H_6-FTIR and C_3H_6-TPD/MS results suggest that the isolated Lewis acid sites ({(≡SiO)$_2$Zn(HO–Si≡)$_2$}) in Zn-MFI can activate the C–H bond of propane and possess weak interactions to propylene, which can avoid cracking and polymerization during PDH reaction. Therefore, the Zn-MFI zeolites exhibit high activity, selectivity, stability, and regeneration ability for PDH. This work presents a convenient and environment-friendly strategy for the preparation of Zn-MFI zeolite. The inspiration from biological processes may bring additional possibilities for the synthesis of other metal-zeolites in an environment-friendly way.

CRediT authorship contribution statement

Xunming Su: Writing – review & editing, Writing – original draft, Validation, Investigation, Formal analysis, Data curation. **Zhong-Pan Hu:** Visualization, Validation, Funding acquisition, Conceptualization. **Jingfeng Han:** Software, Methodology, Funding acquisition. **Yuhong Jia:** Investigation. **Shutao Xu:** Resources, Funding acquisition, Formal analysis. **Jin Zhang:** Formal analysis. **Dong Fan:** Formal analysis. **Yingxu Wei:** Visualization, Validation, Supervision, Funding acquisition. **Zhongmin Liu:** Visualization, Validation, Supervision, Funding acquisition.

Declaration of competing interest

The authors declare that they have no known competing financial interests or personal relationships that could have appeared to influence the work reported in this paper.

Data availability

Data will be made available on request.

Appendix A. Supplementary data

Supplementary data to this article can be found online at https://doi. org/10.1016/j.micromeso.2022.112371.

References

[1] C. Li, G. Wang, Dehydrogenation of light alkanes to mono-olefins, Chem. Soc. Rev. 50 (2021) 4359–4381.
[2] Z. Nawaz, F. Wei, Light-alkane oxidative dehydrogenation to light olefins over platinum-based SAPO-34 zeolite-supported catalyst, Ind. Eng. Chem. Res. 52 (2013) 346–352.
[3] F. Cavani, N. Ballarini, A. Cericola, Oxidative dehydrogenation of ethane and propane: how far from commercial implementation? Catal. Today 127 (2007) 113–131.
[4] S. Chen, X. Chang, G. Sun, T. Zhang, Y. Xu, Y. Wang, C. Pei, J. Gong, Propane dehydrogenation: catalyst development, new chemistry, and emerging technologies, Chem. Soc. Rev. 50 (2021) 3315–3354.
[5] Z. Lian, S. Ali, T. Liu, C. Si, B. Li, D.S. Su, Revealing the janus character of the coke precursor in the propane direct dehydrogenation on Pt catalysts from a KMC simulation, ACS Catal. 8 (2018) 4694–4704.
[6] D. Sanfilippo, I. Miracca, Dehydrogenation of paraffins: synergies between catalyst design and reactor engineering, Catal. Today 111 (2006) 133–139.
[7] Z.-P. Hu, D. Yang, Z. Wang, Z.-Y. Yuan, State-of-the-Art catalysts for direct dehydrogenation of propane to propylene, Chin. J. Catal. 40 (2019) 1233–1254.
[8] K.C. Szeto, B.R. Loges, N. Merle, N. Popoff, A. Quadrelli, H. Jia, E. Berrier, A. De Mallmann, L. Delevoye, R.M. Gauvin, Vanadium oxo organometallic species supported on silica for the selective non-oxidative dehydrogenation of propane, Organometallics 32 (2013) 6452–6460.
[9] P. Castro-Fernández, D. Mance, C. Liu, I.B. Moroz, P.M. Abdala, E.A. Pidko, C. Copéret, A. Fedorov, C.R. Müller, Propane dehydrogenation on Ga$_2$O$_3$-based catalysts: contrasting performance with coordination environment and acidity of surface sites, ACS Catal. 11 (2021) 907–924.

[10] S. Han, D. Zhao, H. Lund, N. Rockstroh, S. Bartling, D.E. Doronkin, J.-D. Grunwaldt, M. Gao, G. Jiang, E.V. Kondratenko, TiO2-Supported catalysts with ZnO and ZrO2 for non-oxidative dehydrogenation of propane: mechanistic analysis and application potential, Catal. Sci. Technol. 10 (2020) 7046–7055.

[11] M. Nadjafi, A.M. Kierzkowska, A. Armutlulu, R. Verel, A. Fedorov, P.M. Abdala, C. R. Müller, Correlating the structural evolution of ZnO/Al2O3 to spinel zinc aluminate with its catalytic performance in propane dehydrogenation, J. Phys. Chem. C 125 (2021) 14065–14074.

[12] W. Qi, P. Yan, D.S. Su, Oxidative dehydrogenation on nanocarbon: insights into the reaction mechanism and kinetics via in-situ experimental methods, Acc. Chem. Res. 51 (2018) 640–648.

[13] L. Shi, Y. Wang, B. Yan, W. Song, D. Shao, A.-H. Lu, Progress in selective oxidative dehydrogenation of light alkanes to olefins promoted by boron nitride catalysts, Chem. Commun. 54 (2018) 10936–10946.

[14] Y. Dai, X. Gao, Q. Wang, X. Wan, C. Zhou, Y. Yang, Recent progress in heterogeneous metal and metal oxide catalysts for direct dehydrogenation of ethane and propane, Chem. Soc. Rev. 50 (2021) 5590–5630.

[15] S. Han, D. Zhao, T. Otroshchenko, H. Lund, U. Bentrup, V.A. Kondratenko, N. Rockstroh, S. Bartling, D.E. Doronkin, J.-D. Grunwaldt, Elucidating the nature of active sites and fundamentals for their creation in Zn-containing ZrO2-based catalysts for nonoxidative propane dehydrogenation, ACS Catal. 10 (2020) 8933–8949.

[16] J. Camacho-Bunquin, P. Aich, M. Ferrandon, U. Das, F. Dogan, L.A. Curtiss, J. T. Miller, C.L. Marshall, A.S. Hock, P.C. Stair, Single-site zinc on silica catalysts for propylene hydrogenation and propane dehydrogenation: synthesis and reactivity evaluation using an integrated atomic layer deposition-catalysis instrument, J. Catal. 345 (2017) 170–182.

[17] N.M. Schweitzer, B. Hu, U. Das, H. Kim, J. Greeley, L.A. Curtiss, P.C. Stair, J. T. Miller, A.S. Hock, Propylene hydrogenation and propane dehydrogenation by a single-site Zn2+ on silica catalyst, ACS Catal. 4 (2014) 1091–1098.

[18] Z.-P. Hu, J. Han, Y. Wei, Z. Liu, Dynamic evolution of zeolite framework and metal-zeolite interface, ACS Catal. 12 (2022) 5060–5076.

[19] Z.-P. Hu, G. Qin, J. Han, W. Zhang, N. Wang, Y. Zheng, Q. Jiang, T. Ji, Z.-Y Yuan, J. Xiao, Y. Wei, Z. Liu, Atomic insight into the local structure and microenvironment of isolated Co-motifs in MFI zeolite frameworks for propane dehydrogenation, J. Am. Chem. Soc. 144 (2022) 12127–12137.

[20] D. Nozik, F.M.P. Tinga, A.T. Bell, Propane dehydrogenation and cracking over Zn/H-MFI prepared by solid-state ion exchange of ZnCl2, ACS Catal. 11 (2021) 14489–14506.

[21] J.A. Biscardi, E. Iglesia, Reaction pathways and rate-determining steps in reactions of alkanes on H-ZSM5 and Zn/H-ZSM5 catalysts, J. Catal. 182 (1999) 117–128.

[22] J.A. Biscardi, G.D. Meitzner, E. Iglesia, Structure and density of active Zn species in Zn/H-ZSM5 propane aromatization catalysts, J. Catal. 179 (1998) 192–202.

[23] S.M. Almutairi, B. Mezari, P.C. Magusin, E.A. Pidko, E.J. Hensen, Structure and reactivity of Zn-modified ZSM-5 zeolites: the importance of clustered cationic Zn complexes, ACS Catal. 2 (2012) 71–83.

[24] A. Mehdad, R.F. Lobo, Ethane and ethylene aromatization on zinc-containing zeolites, Catal. Sci. Technol. 7 (2017) 3562–3572.

[25] X. Niu, J. Gao, Q. Miao, M. Dong, G. Wang, W. Fan, Z. Qin, J. Wang, Influence of preparation method on the performance of Zn-containing HZSM-5 catalysts in methanol-to-aromatics, Microporous Mesoporous Mater. 197 (2014) 252–261.

[26] H. Fan, X. Nie, H. Wang, M.J. Janik, C. Song, X. Guo, Mechanistic understanding of ethane dehydrogenation and aromatization over Zn/ZSM-5: effects of Zn modification and CO2 Co-reactant, Catal. Sci. Technol. 10 (2020) 8359–8373.

[27] C. Chen, Z.-P. Hu, J. Ren, S. Zhang, Z. Wang, Z.-Y. Yuan, ZnO nanoclusters supported on dealuminated zeolite β as a novel catalyst for direct dehydrogenation of propane to propylene, ChemCatChem 11 (2019) 868–877.

[28] L. Qi, Y. Zhang, M.A. Conrad, C.K. Russell, J. Miller, A.T. Bell, Ethanol conversion to butadiene over isolated zinc and yttrium sites grafted onto dealuminated beta zeolite, J. Am. Chem. Soc. 142 (2020) 14674–14687.

[29] L. Xie, R. Wang, Y. Chai, X. Weng, N. Guan, L. Li, Propane dehydrogenation catalyzed by in-situ partially reduced zinc cations confined in zeolites, J. Energy Chem. 63 (2021) 262–269.

[30] Q. Sun, N. Wang, Q. Fan, L. Zeng, A. Mayoral, S. Miao, R. Yang, Z. Jiang, Yu J. Zhou, Subnanometer bimetallic platinum-zinc clusters in zeolites for propane dehydrogenation, Angew. Chem., Int. Ed. 132 (2020) 19618–19627.

[31] D. Zhao, X. Tian, D.E. Doronkin, S. Han, V.A. Kondratenko, J.D. Grunwaldt, A. Perechodjuk, T.H. Vuong, J. Rabeah, R. Eckelt, In situ formation of ZnOx species for efficient propane dehydrogenation, Nature 599 (2021) 234–238.

[32] B. Hu, N.M. Schweitzer, G. Zhang, S.J. Kraft, D.J. Childers, M.P. Lanci, J.T. Miller, A.S. Hock, Isolated FeII on silica as a selective propane dehydrogenation catalyst, ACS Catal. 5 (2015) 3494–3503.

[33] D.M. Kaphan, M.S. Ferrandon, R.R. Langeslay, G. Celik, E.C. Wegener, C. Liu, J. Niklas, O.G. Poluektov, M. Delferro, Mechanistic aspects of a surface organovanadium (III) catalyst for hydrocarbon hydrogenation and dehydrogenation, ACS Catal. 9 (2019) 11055–11066.

[34] S.Q. Zhang, X.F. Yu, H.B. Zhang, N. Peng, Z.X. Chen, Q. Cheng, X.L. Zhang, S. H. Cheng, Y. Zhang, Comparison of the oral absorption, distribution, excretion, and bioavailability of zinc sulfate, zinc gluconate, and zinc-enriched yeast in rats, Mol. Nutr. Food Res. 62 (2018) 1700981.

[35] M.A. Camblor, M.E. Davis, 29Si MAS NMR spectroscopy of tectozincosilicates, J. Phys. Chem. 98 (1994) 13151–13156.

[36] P. Hu, K. Iyoki, H. Yamada, Y. Yanaba, K. Ohara, N. Katada, T. Wakihara, Synthesis and characterization of MFI-type zincosilicate zeolites with high zinc content using mechanochemically treated Si–Zn oxide composite, Microporous Mesoporous Mater. 288 (2019) 109594.

[37] J. Liu, Y. Liu, H. Liu, Y. Fu, Z. Chen, W. Zhu, Silicalite-1 supported ZnO as an efficient catalyst for direct propane dehydrogenation, ChemCatChem 13 (2021) 4780–4786.

[38] L. Wang, S. Sang, S. Meng, Z. Ying, Q. Yue, Z.M. Liu, Direct synthesis of Zn-ZSM-5 with novel morphology, Mater. Lett. 61 (2007) 1675–1678.

[39] Q. Sun, N. Wang, T. Zhang, R. Bai, A. Mayoral, P. Zhang, Q. Zhang, O. Terasaki, J. Yu, Zeolite encaged single atom rhodium catalysts: highly efficient hydrogen generation and shape selective tandem hydrogenation of nitroarenes, Angew. Chem., Int. Ed. 58 (2019) 18570–18576.

[40] F. Goodarzi, L. Kang, F.R. Wang, F. Joensen, S. Kegnæs, J. Mielby, Methanation of carbon dioxide over zeolite encapsulated nickel nanoparticles, ChemCatChem 10 (2018) 1566–1570.

[41] S.V. Konnov, F. Dubray, E.B. Clatworthy, C. Kouvatas, J.P. Gilson, J.P. Dath, D. Minoux, C. Aquino, V. Valtchev, S. Moldovan, Novel strategy for the synthesis of ultra-stable single-site Mo-ZSM-5 zeolite nanocrystals, Angew. Chem., Int. Ed. 132 (2020) 19721–19728.

[42] F. Dubray, E. Dib, I. Medeiros-Costa, C. Aquino, D. Minoux, S. van Daele, N. Nesterenko, J.-P. Gilson, S. Mintova, The challenge of silanol species characterization in zeolite, Inorg. Chem. Front. 9 (2022) 1125–1133.

[43] J. Grand, S.N. Talapaneni, A. Vicente, C. Fernandez, E. Dib, H.A. Aleksandrov, G. N. Vayssilov, R. Retoux, P. Boullay, J.-P. Gilson, V. Valtchev, S. Mintova, One-pot synthesis of silanol-free nanosized MFI zeolite, Nat. Mater. 16 (2017) 1010–1015.

[44] R. Buzzoni, S. Bordiga, G. Ricchiardi, C. Lamberti, A. Zecchina, G. Bellussi, Interaction of pyridine with acidic (H-ZSM5, H-β, H-MORD zeolites) and superacidic (H-nafion membrane) systems: an IR investigation, Langmuir 12 (1996) 930–940.

[45] R.W. Joyner, A.D. Smith, M. Stockenhuber, M.W. van den Berg, The local structure of aluminium sites in zeolites, Phys. Chem. Chem. Phys. 6 (2004) 5435–5439.

[46] M. Orazov, M.E. Davis, Catalysis by framework zinc in silica-based molecular sieves, Chem. Sci. 7 (2016) 2264–2274.

[47] G. Liu, Z.-J. Zhao, T. Wu, L. Zeng, J. Gong, Nature of the active sites of VOx/Al2O3 catalysts for propane dehydrogenation, ACS Catal. 6 (2016) 5207–5214.

[48] F. Dubray, S. Moldovan, C. Kouvatas, J. Grand, C. Aquino, N. Barrier, J.-P. Gilson, N. Nesterenko, D. Minoux, S. Mintova, Direct evidence for single molybdenum atoms incorporated in the framework of MFI zeolite nanocrystals, J. Am. Chem. Soc. 141 (2019) 8689–8693.

[49] B.E. Snyder, P. Vanelderen, M.L. Bols, S.D. Hallaert, L.H. Böttger, L. Ungur, K. Pierloot, R.A. Schoonheydt, B.F. Sels, E.I. Solomon, The active site of low-temperature methane hydroxylation in iron-containing zeolites, Nature 536 (2016) 317–321.

[50] M. Guisnet, N.S. Gnep, F. Alario, Aromatization of short chain alkanes on zeolite catalysts. Aromatization of short chain alkanes on zeolite catalysts, Appl. Catal. A 89 (1992) 1–30.